Radiology Advances, 2024, **1(3)**, umae024
https://doi.org/10.1093/radadv/umae024
Advance access publication: October 25, 2024
Original Research

Magnetic particle imaging enables nonradioactive quantitative sentinel lymph node identification: feasibility proof in murine models

Olivia C. Sehl, PhD, BS[1,2,*], Kelvin Guo, BS[1], Abdul Rahman Mohtasebzadeh, PhD, MS, BS[1], Petrina Kim, BS[1], Benjamin Fellows, PhD, BS[1], Marcela Weyhmiller, PhD, BS[1], Patrick W. Goodwill, PhD, MS, BS[1], Max Wintermark, MD, MS, MBA[3], Stephen Y. Lai, MD, PhD, BS, BA[4], Paula J. Foster, PhD, MS, BS[2], Joan M. Greve, PhD, MS, BS[1]

[1]Magnetic Insight Inc., Alameda, CA 94502, United States
[2]Departent of Medical Biophysics, University of Western Ontario, Robarts Research Institute, London, ON N6A 3K7, Canada
[3]Department of Neuroradiology, University of Texas MD Anderson Cancer Center, Houston, TX 77030, United States
[4]Department of Head and Neck Surgery, University of Texas MD Anderson Cancer Center, Houston, TX 77030, United States
*Corresponding author: Olivia C. Sehl, PhD, BS, Magnetic Insight Inc., 2020 N Loop Rd., Alameda, CA 94502, United States (osehl@magneticinsight.com).

Abstract

Background: Sentinel lymph node biopsy (SLNB) is an important cancer diagnostic staging procedure. Conventional SLNB procedures with ^{99m}Tc radiotracers and scintigraphy are constrained by tracer half-life and, in some cases, insufficient image resolution. Here, we explore an alternative magnetic (nonradioactive) image-guided SLNB procedure.

Purpose: To demonstrate that magnetic particle imaging (MPI) lymphography can sensitively, specifically, and quantitatively identify and map sentinel lymph modes (SLNs) in murine models in multiple regional lymphatic basins.

Materials and Methods: Iron oxide nanoparticles were administered intradermally to healthy C57BL/6 mice (male, 12-week-old, n = 5). The nanoparticles (0.675 mg Fe/kg) were injected into the tongue, forepaw, base of tail, or hind footpad, then detected by 3-dimensional MPI at multiple timepoints between 1 hour and 4 to 6 days. In this mouse model, the SLN is represented by the first lymph node draining from the injection site. SLNs were extracted to verify the MPI signal ex vivo and processed using Perl's Prussian iron staining. Paired *t*-test was conducted to compare MPI signal from SLNs in vivo vs. ex vivo and considered significant if $P < .05$.

Results: MPI lymphography identified SLNs in multiple lymphatic pathways, including the cervical SLN draining the tongue, axillary SLN draining the forepaw, inguinal SLN draining the tail, and popliteal SLN draining the footpad. MPI signal in lymph nodes was present after 1 hour and stable for the duration of the study (4-6 days). Perl's Prussian iron staining was identified in the subcapsular space of excised SLNs.

Conclusion: Our data support the use of MPI lymphography to specifically detect SLN(s) using a magnetic tracer for a minimum of 4 to 6 days, thereby providing information required to plan the SLN approach in cancer surgery. As clinical-scale MPI is developed, translation will benefit from a history of using iron-oxide nanoparticles in human imaging and recent regulatory-approvals for use in SLNB.

Keywords: sentinel lymph node, lymphography, surgical planning, magnetic particle imaging, vivotrax, pharmacokinetics, quantitative, iron oxide nanoparticles

Abbreviations

3D = 3-dimensional, EMA = European Medicines Agency, FDA = Food and Drug Administration, HNC = head and neck cancer, ID = injected dose, LN = lymph node, MRI = magnetic resonance imaging, MPI = magnetic particle imaging, PPB = Perl's Prussian Blue, RRI = Robarts Research Institute, SLN = sentinel lymph node, SLNB = sentinel lymph node biopsy, SPION = superparamagnetic iron oxide nanoparticle

Summary

Magnetic particle imaging enables unambiguous identification of sentinel lymph node locations in multiple mouse lymphatic pathways up to several days following intradermal injection of iron oxide nanoparticles.

Key Results

- Magnetic particle imaging (MPI) specifically visualized sentinel lymph nodes in multiple lymphatic pathways following intradermal injection of iron oxide nanoparticles at various anatomical locations.
- MPI enables stable detection and quantification of iron oxide in lymph nodes at least 4 to 6 days after injection.
- MPI has sufficient sensitivity (50 ng Fe) and shine-through resolution (<3.5 mm) to identify mock lymph nodes in phantoms.
- Iron oxide accumulation in excised lymph nodes was verified using Perl's Prussian blue stain.

Received: July 10, 2024; **Revised:** October 14, 2024; **Accepted:** October 18, 2024

Introduction

Lymph node (LN) metastasis is a critical prognostic factor with therapeutic implications for solid tumors, including head and neck cancer (HNC), melanoma, and breast cancer, among many others.[1–3] Sentinel lymph nodes (SLNs) are any lymph node(s) that receive lymph drainage directly from a tumor site. SLN biopsy (SLNB) has emerged as a diagnostic staging procedure that involves removal of 1 to 4 SLNs, which then undergo evaluation by histopathology to detect disease metastasis.[4] SLNB provides vital information for clinical decision-making, influencing surgery and radiotherapy plans, while significantly reducing patient morbidity compared to complete LN dissection, which represents overtreatment for many patients.[1–5]

A primary challenge for SLNB is identification of SLNs to guide surgical excision.[1,2,4,6] The standard of care for SLN identification is peritumoral injection of ^{99m}Tc-based tracer that drains and accumulates at SLNs allowing for presurgical localization of SLNs by scintigraphy. The technology is limited, however, by short tracer half-life that demands clinical coordination between the injection, imaging technicians, radiologist, operating room, and surgeon(s). Additionally, the accuracy of SLNB is reduced when the injection site is located nearby the draining SLN due to low scintigraphy resolution (shine-though phenomenon).[1,2]

An emerging alternative SLNB guidance procedure, approved by the Food and Drug Administration (FDA) and European Medicines Agency (EMA), uses non-radioactive (shelf-stable) carboxydextran-coated iron oxide nanoparticles to label SLNs, allowing for intraoperative detection of magnetized SLNs using a real-time magnetometer probe. This magnetic technique has been widely adopted for breast cancer SLNB procedures[7–9] and is shown to be noninferior to ^{99m}Tc-based detection methods.[10,11] However, it is currently approved only for patients undergoing mastectomy or lumpectomy[12] because of the well-mapped lymphatic pathways from the breast to the axillary SLN basin. The approved magnetic technique does not currently provide presurgical imaging of SLN locations and therefore cannot be used for complex cancers where SLN drainage pathways can vary, and for cancers affecting complex anatomies with unpredictable and/or multiple nodal basins.[1,2,4,6,13]

Magnetic particle imaging (MPI) is an emerging technology that produces images of the 3-dimensional (3D) distribution of superparamagnetic iron oxide nanoparticles (SPIONs) in vivo. Unlike SPION-based magnetic resonance imaging (MRI), MPI does not have background signal or interference from surrounding tissue and is linearly quantitative, which has enabled numerous applications.[14,15] The purpose of this study is to demonstrate that MPI can identify and map SLNs in murine models and to characterize the pharmacokinetics of SPIONs when administered in multiple regional lymphatic basins.

Materials and methods

Murine SLN model

Although the term "sentinel lymph node" is typically used in the context of cancer, initially using healthy mice allows for the investigation of lymphatic drainage patterns and the assessment of novel SLN mapping techniques without the confounding factors associated with tumor-induced lymphatic remodeling.[16] In this work, the surrogate for the SLN is the first LN along the lymphatic draining pathway from the injection site. For this study, we used naïve, immunocompetent C57BL/6 male mice aged 12 weeks (Charles River, Wilmington, MA) to study transport to draining LNs.[17–20] Three mice were obtained at Robarts Research Institute (RRI) and cared for under standards of Western University Council on Animal Care with an approved protocol. An additional 2 mice were obtained at Magnetic Insight Inc. with an approved protocol by the Institutional Animal Care and Use Committee provided by In Vivo Strategies.

In vivo MPI lymphography

For in vivo lymphography, carboxydextran-coated SPIONs (VivoTrax, Magnetic Insight Inc., Alameda, CA) were administered by intradermal injection at 0.675 mg of Fe/kg (in 50 µL saline), which was scaled by weight from the dose approved for humans (56 mg of Fe/injection).[12] For the 3 mice at RRI, injections occurred at the base of the tail on the right side (n = 1) or tongue (n = 2). Then, 3D MPI at RRI was performed at +1 hour, +48 hours, and +96 hours after injection with imaging parameters described in the following section. For the 2 mice at Magnetic Insight, SPIONs were administered in the left hindpaw (n = 1) or left forepaw (n = 1). Then, 3D MPI at Magnetic Insight was performed at +1 hour, +24 hours, +48 hours, and +144 hours after injection with imaging parameters described later.

MPI was acquired using 2 MOMENTUM scanners (Magnetic Insight Inc.), either at RRI or Magnetic Insight. The 3D acquisitions were performed with the following parameters: field of view = 12 × 6 × 6 cm, transmit axes = x and z (multichannel imaging), gradient strength = 5.7 T/m, radiofrequency amplitude x = 20 mT and z = 23 mT (Magnetic Insight) or 26 mT (RRI), number of projections = 35, reconstruction = Filtered BackProjection, scan time = 35 minutes.

MPI analysis and quantification

From each 3D tomographic dataset, an optimal image slice was used for display that included the injection site and maximum signal from the draining LN. Analysis was performed in MagImage software (Magnetic Insight, Inc.) by O.C.S. (>4 years of experience with MPI quantification). For anatomical context, an optical photograph taken by the integrated camera on the Momentum MPI system was used and a manual tracing of mouse position was overlaid to MPI images.

For MPI signal quantification, first, the maximum signal value was determined from all image slices containing MPI signal of interest. A threshold value ≥ (0.5 × maximum signal value) was used to define a 3D region of interest.[21] Then, the MPI signal was measured as the sum of voxel intensities included in each region of interest.

For each timepoint, in vivo MPI signal in the LN was normalized to the baseline/initial MPI signal to calculate % injected dose (Equation 1). Baseline signals include both the injection site and LN signal at the earliest imaging timepoint (complete at 1 hour).

$$\%\ \mathbf{ID} = \frac{\mathbf{MPI\ signal\ in\ LN}}{\mathbf{Baseline\ MPI\ signal}} * 100\% \qquad \text{Eq.1}$$

For absolute quantification of SPIONs in vivo, the relationship between MPI signal and iron mass was determined.

Multiple calibration samples of VivoTrax (1.25–30.0 µg Fe) were imaged by MPI at each institute. Linear equations derived from the calibration curve phantoms were used to calculate iron content in LNs in vivo (Figure S1).[21,22]

Ex vivo SLN verification

To verify MPI signals ex vivo, mice were euthanized following the last imaging session. SLNs were excised then reimaged by MPI using the same parameters described previously. LNs were imaged ex vivo as freshly harvested tissues and again after fixation in 4% paraformaldehyde. To verify iron in SLNs, fixed LNs were paraffin embedded and sectioned as pairs of 5-µm sections (Zyagen Histology Services, San Diego, CA; or RRI Molecular Pathology Department), then adjacent sections were stained with hematoxylin-eosin (H&E) or Perl's Prussian blue (PPB) (ab245880 and ab150674, respectively; Abcam, Waltham, MA).

MPI LN imaging system verification studies using phantoms

We performed phantom studies to verify MPI sensitivity, linearity, and shine-through (resolution) in the context of mouse LN imaging nearby an injection site. For a 20-g mouse, an injection site is represented by 13.5 µg Fe (0.675 mg Fe/kg dose).

The sensitivity phantom consisted of ten dilutions of VivoTrax (5.5 mg/mL, Magnetic Insight Inc.), from 25 to 800 ng Fe in a volume of 7 µL. These concentrations represent 0.2% to 6% injection dose (ID). The limit of detection was defined as the lowest quantity of iron that produced MPI signal that exceeded 5 times the standard deviation of background noise.

The resolution phantom comprised a central source of 13.5 µg VivoTrax and 6 variably spaced satellite vials containing 675 ng VivoTrax (5% ID). Each well was 1.5 mm in diameter and had a center-to-center spacing of 2.5 to 20 mm from the central source. Line profiles were drawn through MPI signals to measure shine-through resolution limits.

Statistical analyses

A linear regression was performed between VivoTrax quantity (µg) vs. quantified MPI signal for calibration curves. A paired *t*-test was conducted to test for differences in MPI signal from LNs in vivo vs. ex vivo. Analyses were performed with Graphpad Prism 10.1.1 and were considered significant if $P < .05$.

Results

In vivo MPI lymphography

We demonstrated in vivo MPI lymphography can reveal the drainage pattern of VivoTrax injected at multiple lymphatic basins and longitudinal accumulation in SLNs (Figure 1). From the hindpaw, MPI signal was first detected in the ipsilateral popliteal LN (Figure 1A, coronal view). From the base of the tail, MPI signal was first demonstrated in the ipsilateral inguinal LN (Figure 1B, coronal view). From the forepaw, MPI signal was found in the ipsilateral axillary LN (Figure 1C, sagittal view). For mice with tongue injections (n = 2), the MPI signal was first shown in bilateral cervical LNs with a predominant signal in the left node (Figure 1D, coronal view), and a small amount in the lungs because of aspiration of residual tracer. For all mice, some low-intensity background MPI signal was observed in the gastrointestinal region because of iron in mouse feed; no MPI signal was detected from mouse blood or urine (Figure S2).

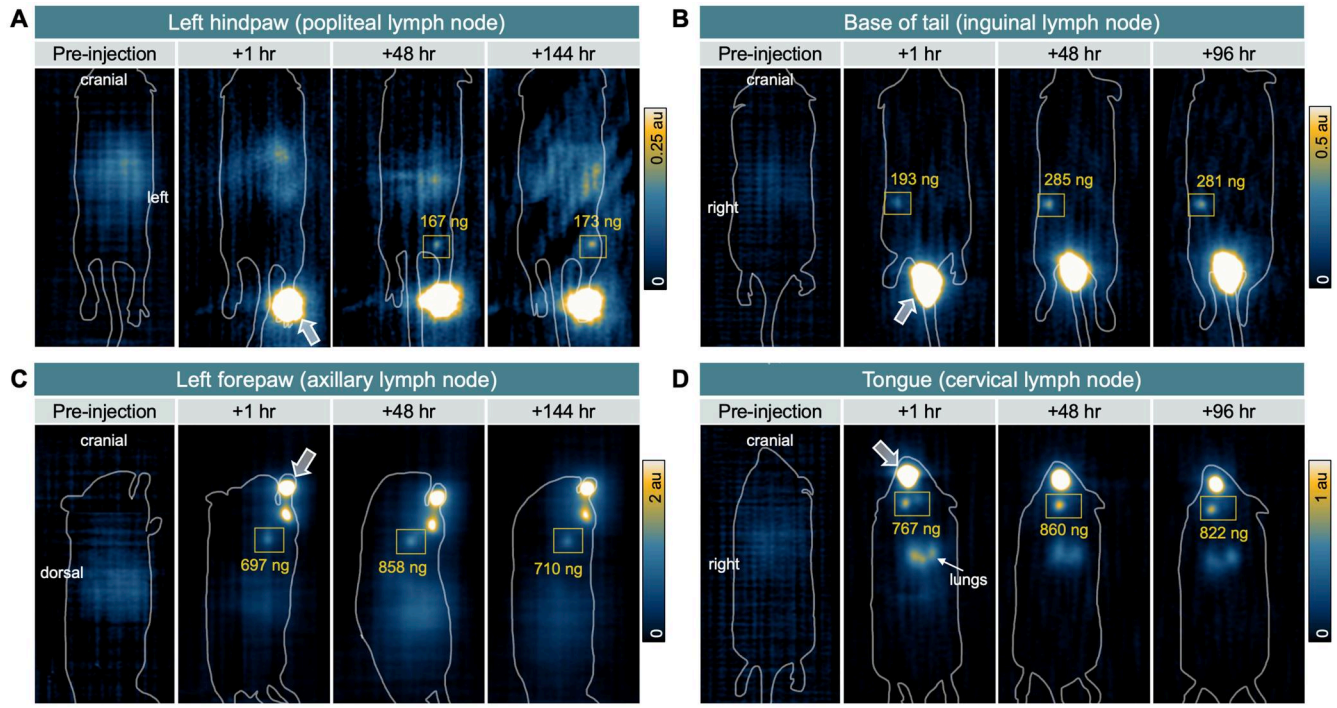

Figure 1. Magnetic particle imaging (MPI) shows in vivo pharmacokinetics of iron oxide nanoparticles to sentinel lymph nodes (SLN) of C57 immunocompetent mice. MPI was acquired preinjection to assess mouse background signal then at 3 timepoints following intradermal injection of VivoTrax to the (A) left hindpaw, (B) right base of tail, (C) left forepaw, and (D) tongue. Arrows indicate location of injection sites. Sentinel lymph nodes are outlined by squares, including the (A) ipsilateral popliteal lymph node, (B) inguinal lymph node, (C) axillary lymph node, and (D) cervical lymph node(s), respectively. Absolute quantification of iron at each lymph node is indicated. A, B, and D are coronal views, whereas imaging of the forepaw required positioning the mouse on its side, resulting in a sagittal view.

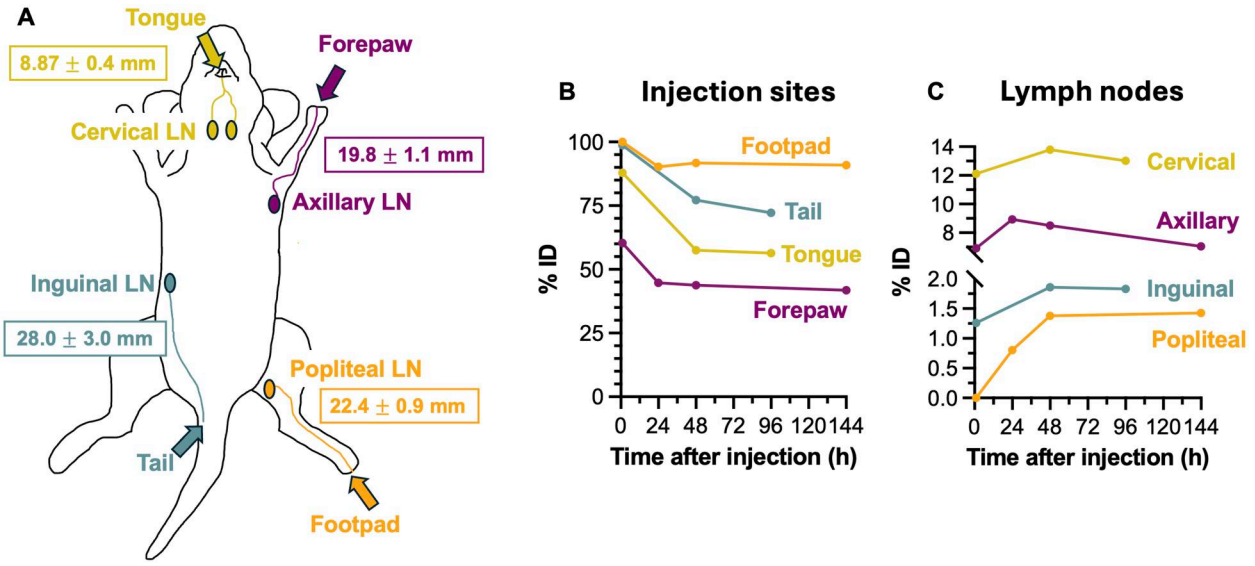

Figure 2. Measurements of distance and pharmacokinetics of iron from injection site to draining lymph nodes, corresponding with magnetic particle imaging (MPI) data in Figure 1. (A) Cartoon showing lymphatic basins draining from the mouse tongue, forepaw, base of tail, and footpad, to the cervical, axillary, inguinal, and popliteal lymph nodes, respectively. The average distance between the injection site and draining lymph nodes, measured from MPI images, is reported (mean ± standard deviation). (B) Longitudinal quantification of MPI signal at the injection site and SLNs for each lymphatic pathway, expressed as percent injected dose (% ID), from 1 hour up to 96 or 144 hours.

The average distances between injection sites and LNs measured from longitudinal MPI are depicted in Figure 2A. Quantification of MPI signal expressed as % ID for injection sites and LNs over time reveals differential pharmacokinetics of SPIONs to LNs depending on injection site (Figure 2B). In all mice, MPI signal at the injection site decreased over time and signal in SLNs persisted for at least 4 to 6 days. The maximum quantified iron (% ID) in popliteal LN was 173 ng (1.4%), inguinal LN was 285 ng (1.9%), axillary LN was 901 ng (8.9%), and cervical LN was 860 ng (13.8%).

Ex vivo SLN verification

Excised LNs were reimaged by MPI and verified in vivo MPI signal (Figure 3A). Quantified MPI signals of LNs in vivo vs. ex vivo were not statistically different ($P = .07$, $n = 5$). A comparison of MPI signal from freshly excised vs. fixed LNs is shown in Figure S3.

Excised LNs were stained with hematoxylin-eosin for general morphology, and Perl's Prussian blue to identify iron (Figure 3B). Iron staining was identified at the periphery of all SLNs in the subcapsular space and LN sinuses.

MPI LN imaging system verification studies using phantoms

MPI sensitivity phantom demonstrated a limit of detection of 50 ng, representing 0.4% mock ID (Figure 4A). A linear relationship was confirmed between VivoTrax iron mass (ng) and measured MPI signal ($R^2 = 0.99$, $P < .001$). Similarly, MPI calibration performed for higher VivoTrax concentrations (1.25–30 μg) showed strong linear relationships with MPI signal at both RRI and Magnetic Insight ($R^2 \geq 0.99$, $P < .001$) (Figure S1). The shine-through phantom shows that 2 1.5-mm diameter wells containing 1:20 VivoTrax concentration ratio is resolvable at a 3.5-mm edge-to-edge distance (5 mm center-to-center distance, Figure 4B).

Discussion and conclusion

Cancer staging by SLNB relies on specific identification of cancer-draining SLNs.[1–4] In this study, we demonstrated the feasibility of MPI to identify SLNs labeled by SPIONs in mouse models. The pharmacokinetics of SPIONs to regional LNs was explored in multiple lymphatic pathways that are commonly affected by metastatic cancers including melanoma and HNC.[23] We produced 3D MPI tomographic images that show iron injection sites, including the mouse footpad, tail, forepaw, and tongue, and their expected draining LNs,[17–20] including the popliteal, inguinal, axillary, and cervical LNs, respectively. Magnetically labeled draining LNs were detected and monitored by MPI for 4 to 6 days and subsequently excised to verify iron presence by histology. This data support the use of MPI lymphography to specifically detect the location of SLN(s) using magnetic (non-radioactive) tracers in an extended timing window, thereby facilitating intraoperative identification of SLNs in complex cancers.

MPI offers several advantageous technical features for preoperative SLN imaging in comparison to existing techniques.[2] The use of magnetic tracers, which are shelf-stable and not limited by radioactive half-life, have the potential to streamline SLNB workflows by enhancing accessibility and availability. In this study, we demonstrate that magnetically labeled LNs can be detected for at least 4 to 6 days. This extended detection window offers greater flexibility in scheduling iron injection, imaging, and surgery, while also enabling new possibilities such as image-guided delayed SLNB procedures.[24,25] As we demonstrate with SPION phantoms, MPI is highly sensitive to enable detection of low iron quantities (50 ng VivoTrax) and has excellent resolution of SLNs from injection sites in close proximity (3.5 mm, with 1:20 iron concentration ratio). These technical specifications enable MPI detection of iron-labeled lymph nodes in various lymphatic pathways (Figure 1). Further, we demonstrate MPI is directly quantitative over three orders of magnitude using 2 MPI scanners. Comparatively, MRI can also be used to visualize SPION-labeled SLNs, but negative MRI contrast and iron

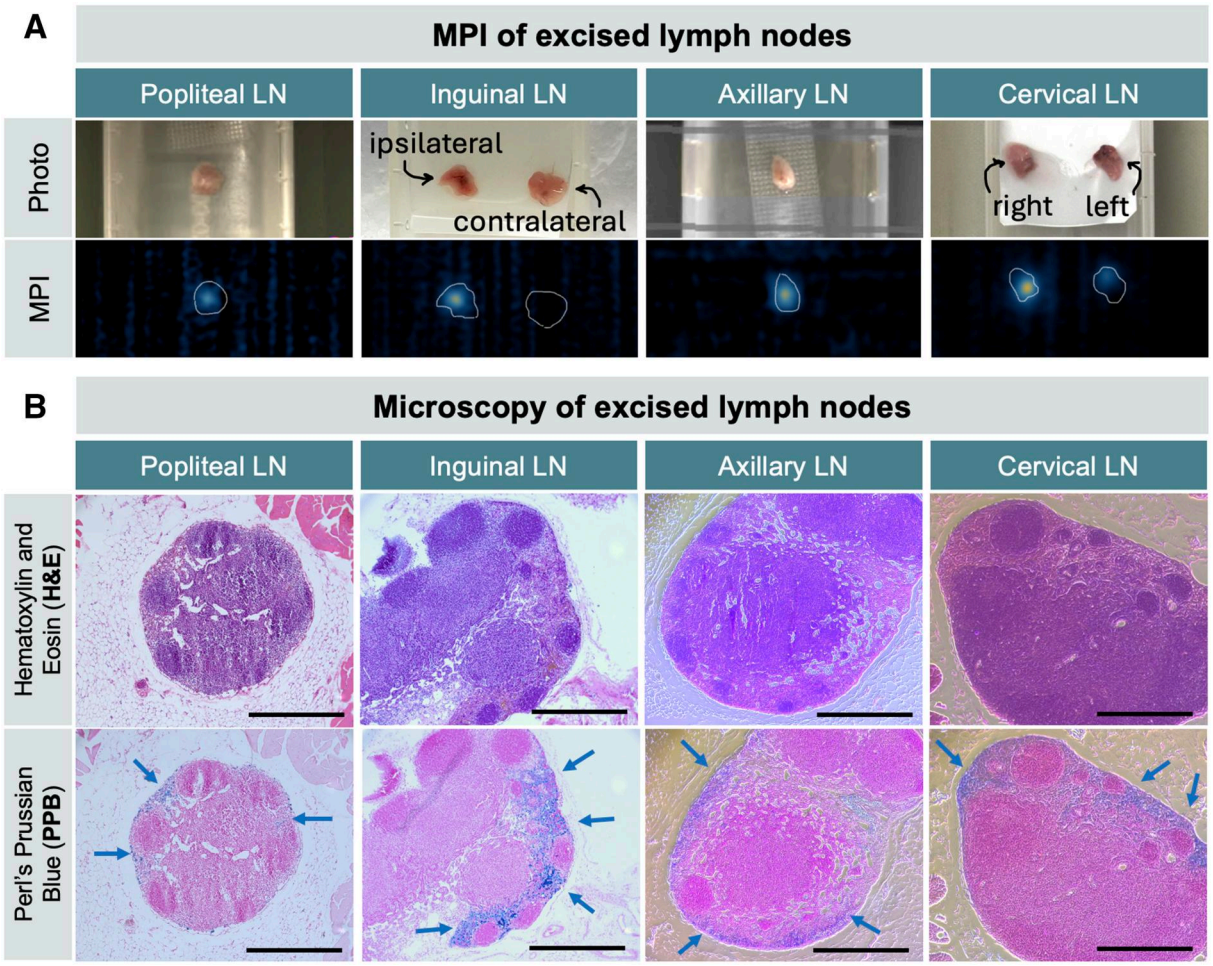

Figure 3. Validation for excised lymph nodes by MPI and histology. (A) MPI of excised tissue verifies that in vivo MPI signal originates from draining lymph nodes. (B) Ex vivo histology of excised popliteal, inguinal, axillary, and cervical lymph nodes including adjacent histopathologic slices with hematoxylin-eosin (H&E) staining (top) and Perl's Prussian blue (PPB) staining (bottom). Iron staining is identified at the periphery of lymph nodes in the subcapsular spaces. Magnification = 10×, scale bars = 0.5 mm.

blooming artifact create ambiguity, leading to challenges for specific SLN identification and quantification.[26–28] Last, MPI provides specific images of SPION-labeled LNs without MPI-detected flow to higher echelon nodes. Rapid leakage of tracer to higher echelon nodes represents a significant limitation for computed tomography-based agents (e.g., iopamidol), gadolinium-based MRI agents, and radiocolloids.[2,26]

We anticipate MPI to be complementary to the intraoperative magnetometer for SLN identification. The current magnetic workflow (Figure 5A, C, D) is FDA- and EMA-approved only for patients undergoing mastectomy or lumpectomy.[12] Adding MPI to the all-magnetic workflow (Figure 5B) has the potential to extend the usability of this technique to other cancer types with complex, multiple potential lymphatic drainage pathways by providing a surgical roadmap for planning the operative approach. For example, use of the magnetic technique is being studied for upper gastrointestinal cancers and HNC, where multiple SLNs may be encountered (NCT05899985).[2,26–28] MPI could provide surgeons with information on the location of SLNs to determine the optimal incision site and anatomic route for excision.

Intraoperative magnetometers provide numerical counts to guide the surgeon to determine the number of SLN(s) to biopsy. For breast cancer, SLNB is complete when residual counts in the axilla are <10% relative to the largest ex vivo reading from an excised SLN (i.e., "10% rule").[10] This is an iterative surgical process.[4] In this work, we demonstrated that MPI can be used for quantification of iron deposition in SLNs in vivo and ex vivo. Therefore, MPI can be used to determine SLN location and quantitate how many SLNs should be excised before surgery (using 10% rule), to direct and simplify the surgical process. Further, our MPI data show differential iron pharmacokinetics to different SLNs. For example, the maximum iron deposition was measured in mouse cervical LNs (~12%–14% ID) and lowest in popliteal LNs (~1%–2% ID), which may be related to lymphatic channel distance (Figure 2A) and/or volume of each SLN.[29] This provides essential knowledge for translating the magnetic SLNB technique to other cancer types involving various lymphatic pathways. In the future, clinical utility of in vivo iron quantification may be explored by correlating iron quantity in SLNs from MPIs with nodal status.[30,31]

Although the current study provides the first feasibility data for SLN imaging with MPI in mouse models, it is limited by low sample sizes in naïve mice. This study motivates future preclinical MPI lymphography involving cancer mouse

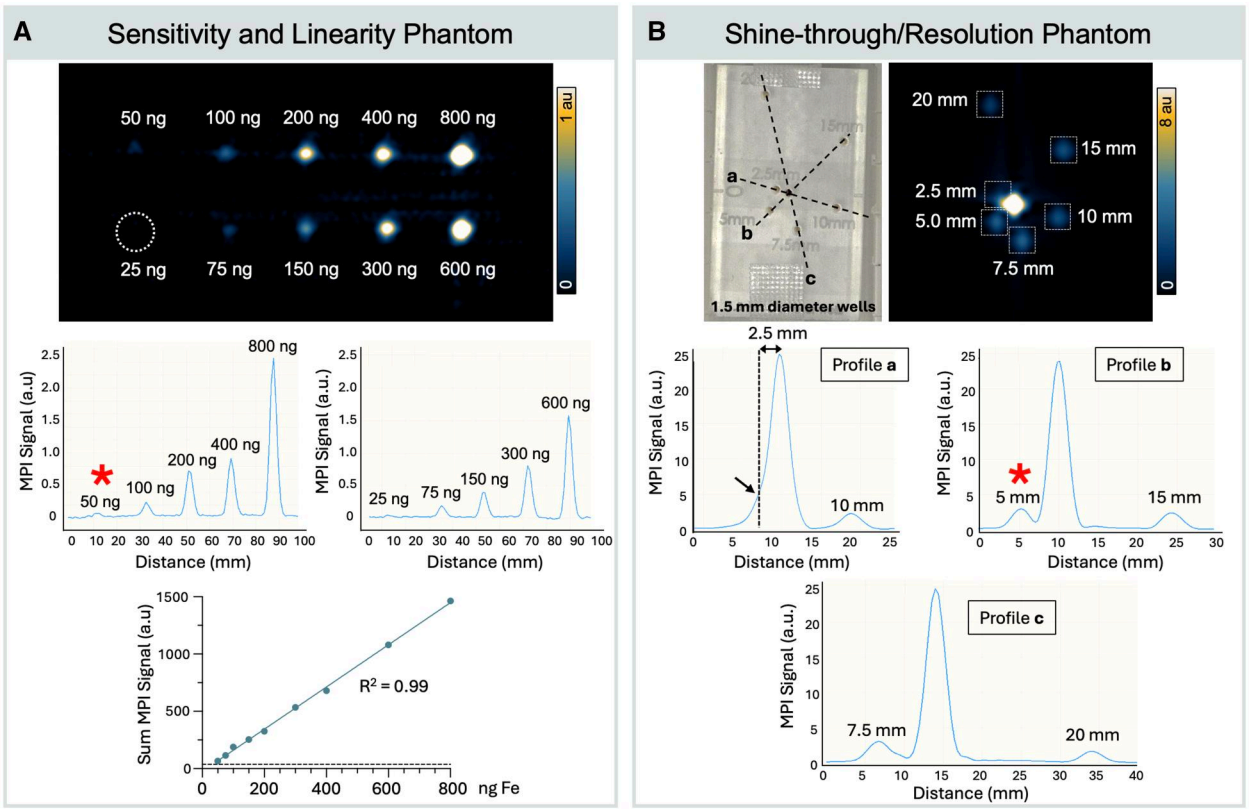

Figure 4. Assessment of preclinical magnetic particle imaging (MPI) technical specifications for sentinel lymph node imaging. (A) Sensitivity and linearity MPI phantom. Three-dimensional MPI of 10 vials with Fe quantities of 25, 50, 75, 100, 150, 200, 300, 400, 600, 800 ng in 7 µL, displayed with window/level = 1/0.5 au. The white dotted line represents the position of the 25-ng VivoTrax sample, which did not meet MPI detection criteria. The limit of detection was determined as 50 ng. Line profiles drawn through MPI signal peaks show signal intensities of each sample and integrated MPI signal is directly linear with Fe quantity ($R^2 = 0.99$). (B) Shine-through/resolution MPI phantom. Three-dimensional MPI of a center vial containing 13.5 µg Fe and satellite vials of 675 ng are 2.5 mm to 20 mm from the source (well center-to-center distance). Phantom wells were 1.5 mm in diameter. MPI is displayed with window/level = 8/4 au. Line plots through MPI signals show that a 675-ng sample can be resolved at 3.5 mm edge-to-edge distance from center vial (5 mm center-to-center distance). Red asterisk (*) indicates the limit of detection (A) and the limit of resolution (B).

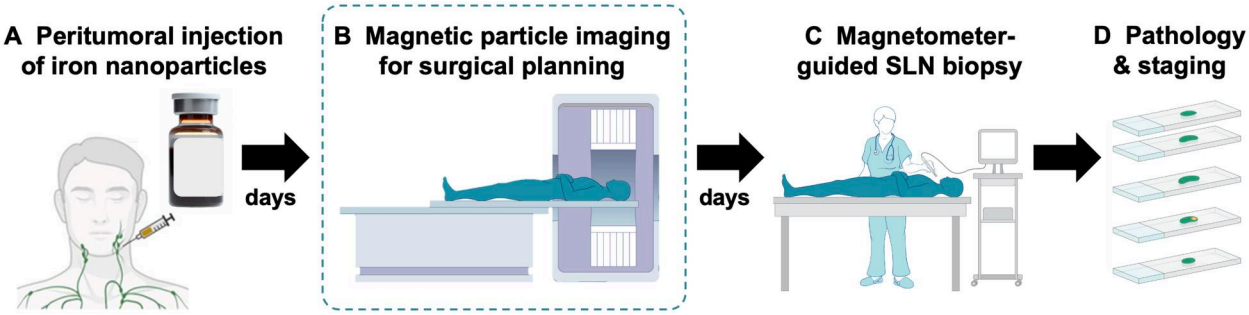

Figure 5. Proposed clinical all-magnetic sentinel lymph node biopsy (SLNB) workflow. (A) First, an iron oxide nanoparticle tracer is administered adjacent to a tumor. (B) A magnetic particle imaging (MPI) scan is acquired before surgery to identify the location and number of SLNs draining from a primary tumor. Provided the data from this study, this image could be acquired hours to days after iron injection, which provides tremendous clinical flexibility. (C) As currently practiced, the surgery could be guided by a magnetometer in real time and (D) excised SLNs would be sent for pathology and staging.

models (e.g., melanoma, HNC). While this study was performed using a preclinical MPI system, there are currently multiple human-scale MPI scanners under development.[32–35] As clinical-scale MPI is developed, translation will benefit from a history of using iron-oxide nanoparticles in human imaging and recent FDA approvals for use in SLNB.[12]

In conclusion, this study is a critical first step toward the development of MPI lymphography using SPIONs for SLNB, particularly for cancers with complex or unpredictable lymphatic drainage patterns. We demonstrated that MPI is a sensitive, quantitative, 3D tomographic imaging technique that specifically identifies SLNs in multiple murine lymphatic pathways over 4 to 6 days. The persistence of MPI signal in LNs for several days provides flexibility and new opportunities for SLNB workflows.

Author contributions

Olivia Sehl (Conceptualization, Data curation, Formal analysis, Investigation, Methodology, Project administration,

Software, Supervision, Validation, Visualization, Writing—original draft, Writing—review & editing), Kelvin Guo (Investigation, Validation, Writing—review & editing), A. Rahman Mohtasebzadeh (Formal analysis, Methodology, Software, Validation, Visualization, Writing—review & editing), Petrina Kim (Investigation, Validation, Writing—review & editing), Benjamin Fellows (Conceptualization, Investigation, Methodology, Visualization, Writing—original draft, Writing—review & editing), Marcela Weyhmiller (Conceptualization, Writing—review & editing), Patrick Goodwill (Conceptualization, Data curation, Funding acquisition, Resources, Software, Validation, Writing—review & editing), Max Wintermark (Conceptualization, Writing—review & editing), Stephen Lai (Conceptualization, Writing—review & editing), Paula Foster (Conceptualization, Funding acquisition, Methodology, Resources, Supervision, Validation, Writing—review & editing), Joan Greve (Conceptualization, Data curation, Funding acquisition, Investigation, Methodology, Project administration, Resources, Supervision, Validation, Visualization, Writing—review & editing)

Supplementary material

Supplementary material is available at *Radiology Advances* online.

Funding

Research reported in this publication was supported by the National Cancer Institute (NCI) and National Institute of Biomedical Imaging and Bioengineering (NIBIB) of the National Institutes of Health under award numbers R44CA285064, 1R44EB035078, R44EB029877. The content is solely the responsibility of the authors and does not necessarily represent the official views of the National Institutes of Health.

Conflicts of interest

Please see ICMJE form(s) for author conflicts of interest. These have been provided as supplementary materials.

Authors O.C. Sehl., K. Guo, A.R. Mohtasebzadeh, P. Kim, B. Fellows, M. Weyhmiller, P.W. Goodwill, and J.M. Greve are employees of Magnetic Insight Inc.

Data availability

The data underlying this article will be shared on reasonable request to the corresponding author.

References

1. de Bree R, de Keizer B, Civantos FJ, et al. What is the role of sentinel lymph node biopsy in the management of oral cancer in 2020? *Eur Arch Otorhinolaryngol*. 2021;278(9):3181-3191.
2. Mahieu R, de Maar JS, Nieuwenhuis ER, et al. New developments in imaging for sentinel lymph node biopsy in early-stage oral cavity squamous cell carcinoma. *Cancers (Basel)*. 2020;12(10):3055.
3. Parrett BM, Kashani-Sabet M, Singer MI, et al. Long-term prognosis and significance of the sentinel lymph node in head and neck melanoma. *Otolaryngol Head Neck Surg*. 2012;147(4):699-706.
4. Bluemel C, Herrmann K, Giammarile F, et al. EANM practice guidelines for lymphoscintigraphy and sentinel lymph node biopsy in melanoma. *Eur J Nucl Med Mol Imaging*. 2015;42(11):1750-1766.
5. de Veij Mestdagh PD, Schreuder WH, Vogel WV, et al. Mapping of sentinel lymph node drainage using SPECT/CT to tailor elective nodal irradiation in head and neck cancer patients (SUSPECT-2): a single-center prospective trial. *BMC Cancer*. 2019;19(1):1110-1119.
6. Leong SP. Detection of melanoma, breast cancer and head and neck squamous cell cancer sentinel lymph nodes by Tc-99m Tilmanocept (Lymphoseek®). *Clin Exp Metastasis*. 2022;39(1):39-50.
7. Lorek A, Stojčev Z, Zarębski W, Kowalczyk M, Szyluk K. Analysis of postoperative complications after 303 sentinel lymph node identification procedures using the SentiMag® method in breast cancer patients. *Med Sci Monit*. 2019;25:3154-3160.
8. Mok CW, Zheng Q, Shi L, Tan SM. Abstract P3-03-26. Challenging dual modality as the gold standard for sentinel lymph node biopsy in breast cancer: a systematic review and network meta-analysis of novel and conventional techniques. *Cancer Research*. 2019;79(suppl 4):P3-03-26-03.
9. Karakatsanis A, Daskalakis K, Stålberg P, et al. Superparamagnetic iron oxide nanoparticles as the sole method for sentinel node biopsy detection in patients with breast cancer. *Br J Surg*. 2017;104(12):1675-1685.
10. Alvarado MD, Mittendorf EA, Teshome M, et al. SentimagIC: a non-inferiority trial comparing superparamagnetic iron oxide versus technetium-99m and blue dye in the detection of axillary sentinel nodes in patients with early-stage breast cancer. *Ann Surg Oncol*. 2019;26(11):3510-3516.
11. Ghilli M, Carretta E, Di Filippo F, et al. The superparamagnetic iron oxide tracer: a valid alternative in sentinel node biopsy for breast cancer treatment. *Eur J Cancer Care (Engl)*. 2017;26(4):e12385.
12. U.S. Food and Drug Administration. Summary of Safety and Effectiveness Data for Magtrace® and Sentimag® Magnetic Localization System, PMA 160053/S002. 2022. Accessed September 6, 2024. https://www.accessdata.fda.gov/cdrh_docs/pdf16/P160053S002B.pdf
13. Uren RF, Howman-Giles RB, Chung D, Thompson JF. Role of lymphoscintigraphy for selective sentinel lymphadenectomy. Selective sentinel lymphadenectomy for human solid cancer. *Cancer Treat Res*. 2005;15-38.
14. Chandrasekharan P, Kuo R, Fung KLB, et al. Magnetic particle imaging in vascular imaging, immunotherapy, cell tracking, and noninvasive diagnosis. *Mol Imaging*. 2023;2023:4131117.
15. Rivera-Rodriguez A, Rinaldi-Ramos CM. Emerging biomedical applications based on the response of magnetic nanoparticles to time-varying magnetic fields. *Annu Rev Chem Biomol Eng*. 2021;12:163-185.
16. Peek MCL, Saeki K, Ohashi K, et al. Optimization of SPIO injection for sentinel lymph node dissection in a rat model. *Cancers (Basel)*. 2021;13(19):5031.
17. Harrell MI, Iritani BM, Ruddell A. Lymph node mapping in the mouse. *J Immunol Methods*. 2008;332(1-2):170-174.
18. Gogineni A, Caunt M, Crow A, et al. Inhibition of VEGF-C modulates distal lymphatic remodeling and secondary metastasis. *PLoS One*. 2013;8(7):e68755.
19. Melancon MP, Wang Y, Wen X, et al. Development of a macromolecular dual-modality MR-optical imaging for sentinel lymph node mapping. *Invest Radiol*. 2007;42(8):569-578.
20. Kosaka N, Ogawa M, Sato N, Choyke PL, Kobayashi H. In vivo real-time, multicolor, quantum dot lymphatic imaging. *J Invest Dermatol*. 2009;129(12):2818-2822.
21. Sehl OC, Tiret B, Berih MA, Makela AV, Goodwill PW, Foster PJ. MPI region of interest (ROI) analysis and quantification of iron in different volumes. *Int J Magn Part Imaging*. 2022;8(1).
22. Nejadnik H, Pandit P, Lenkov O, Pourmehdi Lahiji A, Yerneni K, Daldrup-Link HE. Ferumoxytol can be used for quantitative magnetic particle imaging of transplanted stem cells. *Mol Imaging Biol*. 2019;21(3):465-472.

23. Luke GP, Myers JN, Emelianov SY, Sokolov KV. Sentinel lymph node biopsy revisited: ultrasound-guided photoacoustic detection of micrometastases using molecularly targeted plasmonic nanosensors. *Cancer Res*. 2014;74(19):5397-5408.
24. Karakatsanis A, Eriksson S, Pistiolis L, et al. SentiNot Trialists Group: Mohammed I, Hersi AF, Jazrawi A, Olofsson H, Stålberg P. Delayed sentinel lymph node dissection in patients with a preoperative diagnosis of ductal cancer in situ by preoperative injection with superparamagnetic iron oxide (SPIO) nanoparticles: the SentiNot study. *Ann Surg Oncol*. 2023;30(7):4064-4072.
25. El Sharouni M-A, Scolyer RA, van Gils CH, et al. Time interval between diagnostic excision-biopsy of a primary melanoma and sentinel node biopsy: effects on the sentinel node positivity rate and survival outcomes. *Eur J Cancer*. 2022;167:123-132.
26. Uemura H, Ota I, Fujii T, et al. Sentinel lymph node detection in patients with oral cancer by MR lymphography using superparamagnetic iron oxide. *TOOTORJ*. 2013;7(1):14-18.
27. Nieuwenhuis ER, Kolenaar B, Hof JJ, et al. A comprehensive grading system for a magnetic sentinel lymph node biopsy procedure in head and neck cancer patients. *Cancers (Basel)*. 2022;14 (3):678.
28. Stijns RC, Philips BW, Nagtegaal ID, et al. USPIO-enhanced MRI of lymph nodes in rectal cancer: a node-to-node comparison with histopathology. *Eur J Radiol*. 2021;138:109636.
29. Maeda T, Yamamoto Y, Furukawa H, et al. Dominant lymph drainage patterns in the occipital and parietal regions: evaluation of lymph nodes in patients with skin cancer of the head. *Int J Clin Oncol*. 2017;22(4):774-779.
30. Johnson L, Pinder SE, Douek M. Deposition of superparamagnetic iron-oxide nanoparticles in axillary sentinel lymph nodes following subcutaneous injection. *Histopathology*. 2013;62(3):481-486.
31. Motomura K, Ishitobi M, Komoike Y, et al. SPIO-enhanced magnetic resonance imaging for the detection of metastases in sentinel nodes localized by computed tomography lymphography in patients with breast cancer. *Ann Surg Oncol*. 2011;18 (12):3422-3429.
32. Mattingly E, Mason E, Sliwiak M, Wald LL. Drive and receive coil design for a human-scale MPI system. *Int J Magn Part Imaging IJMPI*. 2022;8(1 suppl 1).
33. Graeser M, Thieben F, Szwargulski P, et al. Human-sized magnetic particle imaging for brain applications. *Nat Commun*. 2019;10 (1):1936.
34. Vogel P, Ruckert M, Greiner C, et al. iMPI: portable human-sized magnetic particle imaging scanner for real-time endovascular interventions. Sci Rep. 2023;13(1):10472.
35. Mason EE, Barcikowski E, Carl J, et al. Preliminary results: large bore clinical MPI system imaging human head-sized FOVs. *Int J Magn Part Imaging IJMPI*. 2024;10(1 suppl 1).

Radiology Advances, 2024, 1, 1–8
https://doi.org/10.1093/radadv/umae024
Original Research